Active Scour Monitoring using Ultrasonic Time Domain Reflectometry of Buried Slender Sensors

Morgan L. Funderburk[1,2], Jamie Tran[1,2], Michael D. Todd[1], Anton Netchaev[3], and Kenneth J. Loh[1,2]

[1] Department of Structural Engineering, University of California San Diego, La Jolla, CA, USA
[2]Active, Responsive, Multifunctional, and Ordered-materials Research (ARMOR) Lab, University of California San Diego, La Jolla, CA, USA
[3]U.S. Army Engineer Research and Development Center, U.S. Army Corp of Engineers, Vicksburg, MS 39180, USA.

E-mail: kenloh@ucsd.edu

Received xxxxxx
Accepted for publication xxxxxx
Published xxxxxx

Abstract

Local scour is a growing cause of bridge failure in the United States and around the world. In the next century, the effects of climate changes will make more bridges susceptible to scour failure more than ever before. This study aims to harness the spatially continuous monitoring capabilities of ultrasonic time-domain reflectometry to detect a soil interface for the purposes of scour monitoring. In this study, a long, slender plate is coupled with two flexible piezoelectric devices that propagate Lamb waves along the length of the plate to form the scour sensor. The sensor was tested for sensitivity to external pressure using metal weights, and was able to detect the position of the pressure up at a length of up to ~ 20 feet. The sensor was tested under simulated scour conditions, being buried in sand at various depths. The results show that the Lamb wave scour sensor is capable of reliably detecting a soil interface at 1 ft intervals. The scour sensor was also able to detect uncompacted soil interfaces, which is important considering the issue of scour hole refill following an extreme event.

Keywords: Scour monitoring, ultrasonic, time-domain reflectometry, Lamb waves, soil-interface

1. Introduction

A prominent and growing cause of bridge failures worldwide is local scour [1]. Local scour around a bridge pier occurs when fluid downflow at the face of the pier begins to erode sediments at its base, which jeopardizes the integrity of the foundation [2]. During scour, soil at the base of the pier is eroded first by downflow, followed by horseshoe vortices that deepen and widen the scour hole (Fig. 1). Wake vortices to the rear of the pier can also contribute to scour erosion and pushes previously supportive sediments downstream. Furthermore, periods of erosion and infill mean that the presence of less-supportive soil around the base can obscure the severity of scour [3]. Hydraulic failure – failures recorded with descriptions such as hydraulic, flood, scour, tidal, and debris – caused over 55% of all bridge collapses in a 22-year period [4]. In addition, it was found that most hydraulic collapses were a result of scour-induced failure [5,6]. Bridge scour failure is a problem of national scope, as it effects bridges all over the U.S.[7]. Due to climate change causing longer and more intense rainy seasons, it is estimated that, in the next 75 years, 90% of bridges in the Southwestern United States (U.S.)

will become susceptible to scour [8]. Damage to highways and bridges in the U.S. from flooding events were estimated to cost US$100 million per event in repairs, and ~ 25 collapses per year are due to hydraulic failures (*i.e.* ~ US $2.5 billion per year) [1]. Similarly, retrofitting bridges in Europe for scour risk mitigation between 2040 and 2070 is estimated to cost between 380 and 540 million €/year [9]. The USGS notes that in addition to the actual costs of repairs, there are indirect costs associated with the disruption of local economy and the cost of longer commutes in detours in the area of the failed or damaged bridge [7]. Therefore, there is an urgent need to develop and deploy scour monitoring systems for detecting when scour has jeopardized structural safety. In general, early damage detection facilitates more efficient asset management while minimizes repair costs.

Traditional scour monitoring methods suffer from deficiencies on when, and under what conditions, they can collect scour data. Conventional methods, such as physical probing, must be performed by a trained technician [5]. Physical probing can also only be performed on a semi-regular basis based on technician availability and permitting weather conditions. Sonar has offered improvements in a few areas, such as the physical area of monitoring coverage and the regularity in which data can be collected. Unfortunately, boat sonar, which can measure the full topography of a scour hole, still needs to be operated by an on-site technician. Furthermore, all types of sonar systems have difficulty collecting accurate data during severe flow conditions and turbid waters [10]. Therefore, emerging areas of scour research focus on permanently installed monitoring technologies that can collect data continuously, even during severe flow, and without the need of an on-site technician.

For instance, fiber Bragg gratings (FBGs) have been studied for use as scour depth monitoring systems. FBGs use periodic refractive structures embedded within an optical fiber to reflect narrowband wavelength ranges of light, where each reflective band is uniquely designed within the available illumination spectrum to correspond to a specific physical location of the FBG. When an FBG is strained, the periodic refractive structure expands or contracts and proportionally shifts the wavelength of the reflected light, thus conveying local strain information. Using the full available infrared optical spectrum provided by the source, FBGs can be multiplexed within a single optical fiber to collect arrayed strain data from multiple locations along the optical fiber. Scour monitoring using FBG sensors can be achieved by detecting changes in strain at discrete bridge-mounted locations due to water temperature [11], water exposure [12,13], or lateral soil pressure [14]. Other FBG methods monitor changes to a driven-rod by detecting increased levels of strain [11] or shifts in vibration frequency as scour erosion increases exposed length [15].

On the other hand, optical time-domain reflectometry (TDR) has also been employed for detecting scour near buried pipelines. Here, scour would expose portions of the pipe, and the difference in temperature between sand and water causes a Doppler frequency shift in the optical fiber running parallel to the exposed area [16]. The advantage of optical TDR is that the entire length of the optical fiber is available for sensing, as opposed to FBGs that only offer discrete sensing locations at the Bragg gratings. In general, a key advantage of TDR is that they are spatially continuous sensors and can provide information along the entire length of the sensing structure.

Another promising bridge scour monitoring method uses electrical TDR to detect changes in the position of the soil-water interface to deduce scour depth. This mechanism works by detecting reflections due to electrical impedance shifts from changes in the surrounding material [17–21]. Initial applications of electrical TDR for scour and soil-water interface monitoring used solid metal rods, but they suffered from sensor fowling problems and had measurement limitations due to attenuation. There were also issues with outside influences, such as raindrops, which clung to the sensing cable, obscuring the air-water interface, and changing propagation velocity in air. Significant improvements to durability were made using twisted cable systems, which were anchored between the bridge pier and a predetermined subsurface location [22]. This type of system successfully measured scour during a storm event. However, these sensors still faced issues with pull-out failure due to insufficient bottom anchorage and electrical shorts due to abrasion of its insulative polymer coating [23].

In this study, scour monitoring using ultrasonic time-domain reflectometry (UTDR) is proposed, where it leverages TDR's ability to localize features while eliminating issues related to electrical shorts. In fact, UTDR, which is based on propagating ultrasonic waves in structures, has been widely used for structural health monitoring and detecting various forms of damage in beams and plates (*e.g.* cracks, corrosion, and composite delamination) [24–26]. These damage features alter the acoustic impedance landscape within the structure and allow propagating ultrasonic waves to reflect at the damage interface. Damage locations can then be determined based on the wave's time-of-flight and the material's known speed of sound.

In this study, the UTDR sensing mechanism based on propagating Lamb waves in a long, slender, sensing strip was used to determine the location of the soil interface for scour monitoring purposes. Previous work by Funderburk *et al.* [27] utilized MFCs to generate first-order symmetric (S0) Lamb waves for detecting pressurized locations with various interfaces, including sand. However, this earlier test was short-range and did not demonstrate detection of a buried soil interface, as would be seen by a buried UTDR sensor undergoing *in situ* scour. Furthermore, the test involved a 6 ft

(1.8 m) sensing strip, whereas local scour causes erosion that can be up to 10 ft (30 m) or more [28].

Overall, the objective of this study is to demonstrate a proof-of-concept for using UTDR as a viable candidate for scour monitoring. Therefore, this study aimed to demonstrate scalability by extending the sensing strip to be ~ 21 ft (6.4 m) in length, and the UTDR sensing mechanism was validated by placing weights at different positions along the strip. Then, the sensor was tested in a soil box where it was able to be fully surrounded by compacted sand at controlled depths. Furthermore, UTDR was used to evaluate both compacted and uncompacted forms of sand interfaces, as either can be potentially present during scour. Overall, UTDR offers a few distinct advantages for detecting scour, namely, by providing spatially continuous measurements and the ability to detect erosion as well as infill.

2. UTDR Background

2.1 Principles of UTDR

Ultrasonic time-domain reflectometry is a long-used and well-known technique for evaluating the damage in large structures. The UTDR method is based on two principles: (1) the constant speed of sound in homogenous materials and (2) the reflection of sound waves due to shifts in acoustic impedance. Damage cause either a significant shift in material properties (*e.g.* corrosion) or the formation of new impedance boundaries, wherein tiny regions of air serve as the impedance mismatch (*e.g.* cracking, delamination, or extreme cases of corrosion) [24–26].

A pulse-echo setup, where the piezoelectric actuator and sensor are at the same end of the sensing strip, was implemented for scour monitoring using UTDR. In a homogenous material, the time-of-flight (TOF) of a reflected wave is related to the distance as follows:

$$2x = vt \tag{1}$$

where x is the distance between the transducer and the location-of-interest (LOI), v is the phase velocity of the acoustic wave, and t is TOF.

2.2 Lamb waves for UTDR

Surface waves, which interact significantly with the interface between the structure and the surrounding material, show a proclivity to react with changes to the surrounding environment. In particular, Lamb waves, are known to interact with the surrounding material on both the top and bottom sides of a plate structure [29]. Lamb waves produce stresses throughout the thickness of a plate, which is often used for interrogating surface or internal defects in structural components [30,31].

Lamb waves occur in two deflected mode shapes throughout the plate, which are symmetric and asymmetric. Both mode shapes cause deformation on both the top and bottom surfaces, so either shape would theoretically be highly sensitive to changes in the surrounding material. The type of mode shape, as well as the propagation velocity, is dependent on the frequency-thickness product. Frequency is dependent on the input signal to the transducer and the thickness of the plate. Dispersion curves for various thicknesses of steel are widely used and were not uniquely calculated for this study [32,33].

Lamb waves are generally introduced into a structure by a piezoelectric device applied at an angle to the surface of interest [34]. However, macro-fiber composites (MFCs), which are thin, flexible, piezoelectric transducers bonded flush to the structure, could also introduce Lamb waves and are highly durable [35,36]. MFCs are limited by their frequency output, and for most plates they fall below the frequency needed to introduce higher order symmetric or asymmetric modes. However, the introduction of only a single Lamb wave mode could be advantageous and has been shown to be ideal for producing strong response signals without dispersion [34]. Lower frequency Lamb waves are also able to travel longer distances without attenuation, making them suitable for long-range inspections, such as for a long sensing strip as proposed in this study. Furthermore, the group velocity of a single-mode Lamb wave remains constant over a narrow band of frequencies. Consulting the dispersion curves for steel, at very low frequencies (< 1 MHz) and assuming a constant thickness, the symmetric mode has a relatively constant velocity, whereas the asymmetric mode is extremely unstable and increases exponentially with frequency. Therefore, the dispersive nature of Lamb waves can be reduced at low frequencies by exciting only the first symmetric mode shape (S0 mode).

2.3 UTDR for scour depth monitoring

UTDR for scour monitoring will be unique in that the propagating medium does not need to have any permanent damage, but rather impedance changes will stem from where the surrounding soil interface is in contact with the buried sensing strip. Funderburk *et al.* [27] showed that Lamb waves are sensitive to external pressures that interact with the surface. To detect scour, Lamb waves are propagated down the length of a thin strip, which is essentially a plate that is much longer than its width. As the Lamb wave propagates and interacts with the soil interface and the associated pressure, it will cause an impedance change that is significant enough to send a reflected wave from the location of the interface. The distance to the soil interface can be calculated by finding the TOF of the reflection (*i.e.*, using *a priori* knowledge of wave mode and speed). Figure 1 shows the basic principles of the UTDR scour sensing mechanism. As local scour and erosion

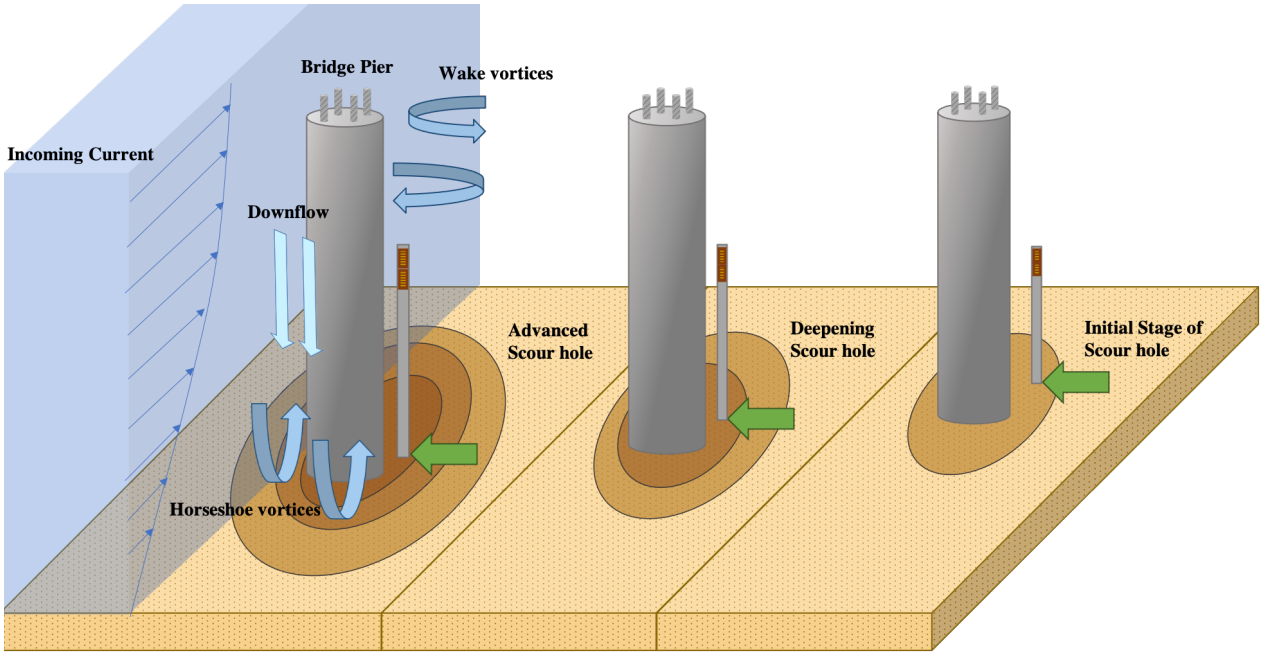

Figure 1. Vortices erode sediment and deepen the scour hole around the base of a bridge pier. As a result, the soil interface moves further down the length of the UTDR sensor.

of sediments near the sensor occur, TOF will increase, thereby allowing the change in scour depth to be calculated.

3. Experimental Details

Typically, transducers produce ultrasonic waves that inspect regions immediately adjacent or below them. For instance, a large plate structure can be inspected using C-Scan, where a longitudinal transducer is moved along the surface of the plate at a fixed distance to look for defects in the plate. C-scan transducers are coupled to the plate in a variety of ways but cannot be permanently attached due to its lateral movement along the surface. Conversely, non-dispersive Lamb waves can be propagated through plates over long distances and are generated by surface mounted transducers, making them ideal for UTDR in plates. For this test, Lamb waves will be introduced into a 1/16 in thick steel strip using MFCs. For the generation of ultrasonic waves, MFCs are actuated to elongate or contract directionally in-plane when voltage is applied. As sensors, they produce voltage when strained in the same manner.

3.1 Sensor design

Previous Lamb wave UTDR work by Funderburk *et al.* [27] validated that an applied metal interface produced a detectable reflected wave response that varied according to the location of the interface. This previous study, however, was performed using an aluminium strip, which is lower in stiffness and could be more sensitive to localized pressure from to a weaker pressure interface, such as soil. For comparison purposes, similar tests were performed using the longer steel strip to reveal any significant sensitivity differences.

Figure 2 shows the sensor design where two M8528-P1 MFCs (Smart Material) were bonded, using double-sided tape (3M), on the same face at one end of a 21 ft long, 1.75 in wide steel strip. The MFCs have an 85 mm (3.3 in) active length and a 25 mm (0.98 in) active width and elongate when a positive voltage is applied. In this case, a pulse-echo system was realized by using one MFC as an actuator and the other as a sensor. While it is possible to use a single sensor for both sensing and actuation, due to their compact size and ease of installation, it was deemed unnecessary to use the switching mechanism necessary to capture the return waveform using just one MFC.

It should be noted that, throughout testing, it was determined that the width of the MFC should match closely with the width of the sensing strip to avoid extraneous wave formation that obscures results. MFCs that are closely matched the width of the strip essentially produce a Lamb wave that propagates in only one direction or dimension (1D), which is down the length of the strip as opposed to the radial direction. Matching the width of the MFCs to the width of the sensor strip follows with the principles of 1D wave propagation, which assumes that stress from the wavefront is applied to the end of a structure with just a single dimension [37]. For the strip to behave as a 1D structure, the wavefront needs to be forced along the *x*-direction by evenly exciting the

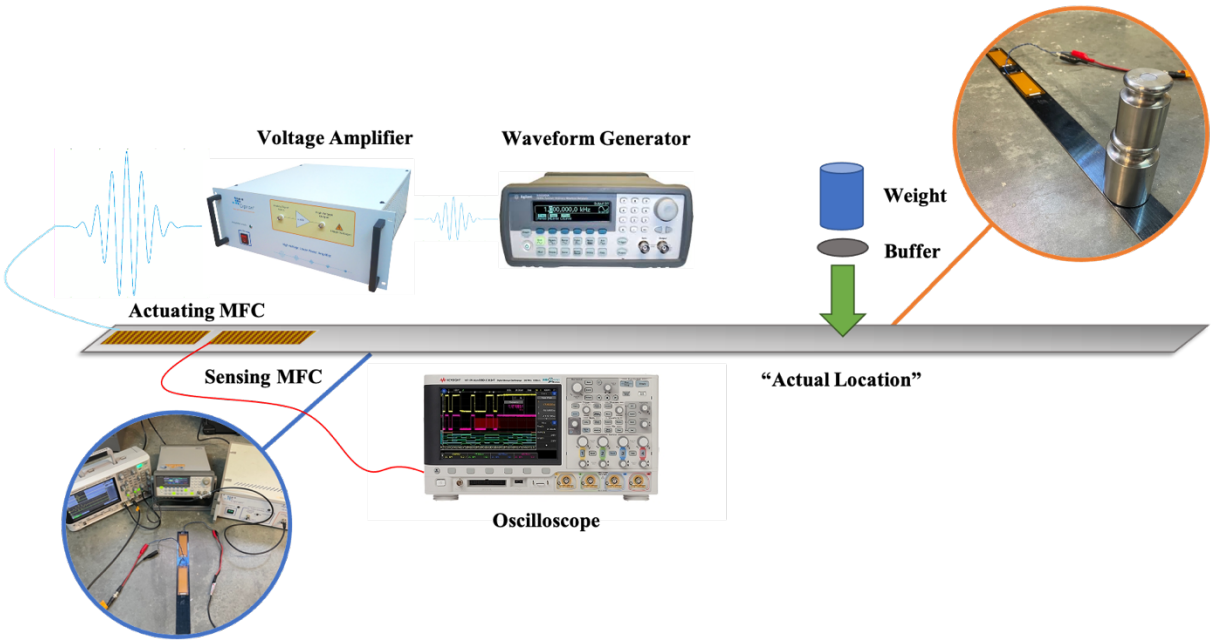

(a)

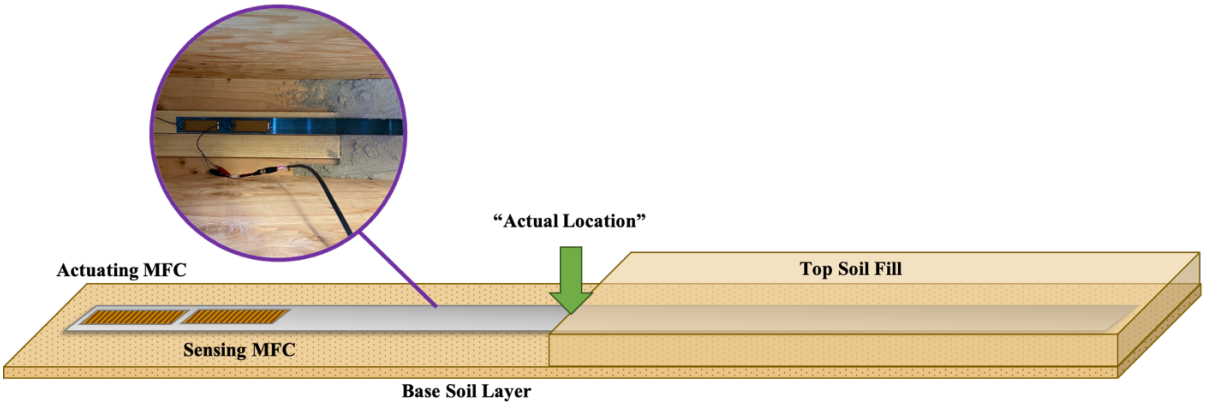

(b)

Figure 2. (a) The UTDR sensor is set up to be tested with weights and (b) with a soil interface.

other two dimensions (*i.e., y* and *z*). If it is assumed that the *z*-direction is the plate thickness (which due to its thinness already exclusively participates in the *x*-direction Lamb mode), then the plate's *y*-direction (*i.e.*, width of the strip) would need to be excited evenly as if to act as a single node.

3.2 Signal generation and data acquisition

First, the MFC actuator was connected to a Ciprian US – TXP – 3 High-Voltage Linear Power Amplifier, which amplifies the input voltage approximately 200× and can handle high-frequency signals between 10 kHz and 10 MHz. The amplifier was connected to an Agilent 33220A Function Waveform generator that outputted a ±500 mV, 7.8-cycle, Gaussian sine wave pulse at a packet frequency of 2.5 kHz, giving it an overall center frequency of approximately 19.5 kHz and an amplified input voltage of ±100V. The center frequency was determined by manually adjusting the packet frequency and selecting the frequency that produced the largest amplitude reflected response.

The excitation waveform plays a critical role in producing a clean Lamb wave signal and therefore a simply analysed reflected response. The actuating MFC was excited using a multi-cycle sine wave packet that is modified by a Hanning window and pulsed every 150 ms to ensure that no interference occurred between consecutive signals [34]. The modified tone burst, rather than a simple sine wave tone burst, reduces the amplitude and therefore the participation of frequencies other than the center frequency. Over long ranges, by limiting the frequency spectrum of the input waveform, the possibility for unwanted dispersion is further reduced.

Second, the sensing MFC received the first pass of the input pulse, as well as the reflected signals from impedance changes

along the length of the steel strip and from the end of the strip. The sensing MFC was connected to a Keysight InfiniiVision DSOX3024T oscilloscope, and the outputted waveform was averaged 30× to reduce noise. Data was stored directly to a USB flash drive as text files containing comma-separated values.

3.3 Localized pressure sensitivity tests

Localized pressure tests were performed using 1500 kg weights placed at 1 ft (30.5 cm) increments along the 21 ft steel sensor strip as diagrammed in figure 2a. The weight was placed between 2 to 20 ft, with the weight location serving as the LOI. The 1 ft location was excluded as it was too close to the sensor and wave reflections would be obscured by the input. The 21 ft location was also excluded because it was the end of the strip. An aluminium washer was used as a buffer between the weight and strip to ensure a fixed contact area and consistent applied pressure. The steel strip was laid flat on a hard concrete surface so as not to induce any unwanted strain into the strip. At each position where the weight was placed, UTDR tests were performed by exciting the MFC actuator and recording the reflected Lamb wave signals using the MFC sensor, as was described in Section 3.2. Once the input voltage was applied, the measured signal was allowed to stabilize visually before the oscilloscope was stopped and the resulting signal was saved to the USB. It should be mentioned that a baseline signal was acquired before any weight was added to the strip.

3.4 Simulated scour tests

Simulated scour tests were conducted using a soil box that was 2 ft (61 cm) wide and 25 ft (7.6 m) long. The box was filled with an even 1 in (2.54 cm) thick base layer of wetted sand. Wetted sand was used to facilitate compaction while also simulating a scour environment. Notably, different soil materials might have different properties governing how ultrasonic energy behaves. Therefore sand might behave differently than other types of soil (*i.e.* clay, silt, etc.). These tests will only show functionality of the UTDR technology when sand is selected as the soil medium.

The sensor strip was placed on top of the leveled sand base layer, and a wooden plank was used to weigh down the end of the sensor strip with MFCs as shown in figure 2b. Once the scour sensor was set into the box, additional sand was added to bury the sensor strip in 1 ft increments up to 20 ft, with the leading edge of the sand being the LOI, which is also referred to as the soil interface. Sand was added rather than removed, which is typical during scour, to prevent disturbing the base sand layer. Newly added sand was always compressed and compacted to ensure an even distribution of applied pressure. The process of adding sand is depicted in figure 3, with the compacted sand shown in figures 3b and 3d. After sand was added to the appropriate level, the excitation signal was applied to the MFC actuator. The response signal was allowed to visually stabilize before the oscilloscope data collection was stopped and the data saved.

In addition, it was of interest to simulate in the laboratory conditions that reflected soil infill post-scour. Therefore, the scour sensor was tested for its ability to detect an uncompacted soil interface commonly found after infill. Infills are typically less compacted and have lower load carrying capacity than the pristine foundation materials. At the same time, many existing scour sensors cannot effectively detect infill. In this case, sand that was added to the soil box was left uncompacted following each fill event. Upon adding sand for the next fill event to bury the sensor strip an additional 1 ft, previously added sand was compacted as shown in figure 3b. This process was repeated as more uncompacted sand was added adjacent to the previous layer, shown in figure 3c, and then compacted as in figure 3d.

(a) (b) (c) (d)

Figure 3. The sand compaction process involved (a) adding a sand layer and (b) then compacting the same sand with distrubuted pressure. (c) Uncompacted sand was added adjacent to the previous top sand fill and measured before being (d) compacted.

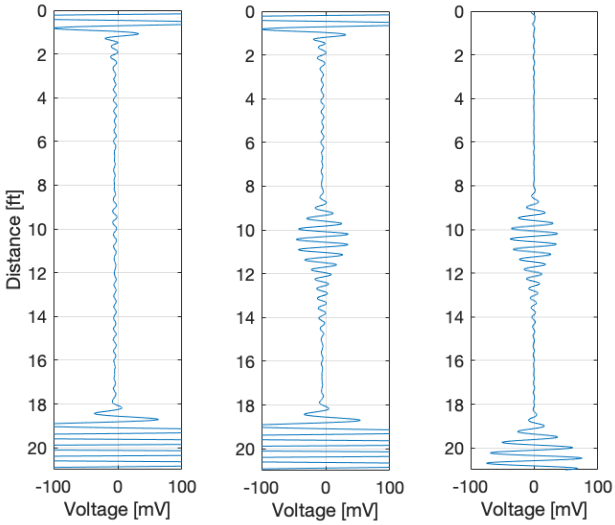

Figure 4. (a) A baseline raw signal without additions is subtracted from (b) a signal from the sensor strip weighted at 10 ft to (c) calculate the final residual signal.

4. Results and Discussion

4.1 Localized pressure results

Localized pressure tests, as described in Section 3.3, were performed to verify that the scour sensor strip could detect changes in the boundary conditions. Figure 4 shows how the measured data was processed for each case (*i.e.*, in this case, when the weight was placed at 10 ft). For visualization purposes, the plots show voltage as a function of distance rather than time. The *y*-axis distance was calculated using equation 1 by multiplying the time value by the known velocity of the Lamb wave in the steel strip, which is in this case 5000 m/s.

The experimental data was then processed by subtracting the baseline signal, as shown in figure 4a, from the measured signals, which is shown in figure 4b, (*i.e.*, with the weight), to obtain the corresponding residual signal in figure 4c. Only the signal representing the time between the first pulse and the first end-of-beam return pulse was analyzed in this study. However, it should be mentioned that an unburied strip saw more than 10 end-of-beam reflections, meaning that the wave generated is able to propagate over 400 ft and still be detected by the MFC sensor. Subtracting the baseline signal allows the residual signal to show a clear reflection at the LOI. In addition, there exists an inverted reflection signal at the end of the strip. The inversion and reduction in amplitude of the

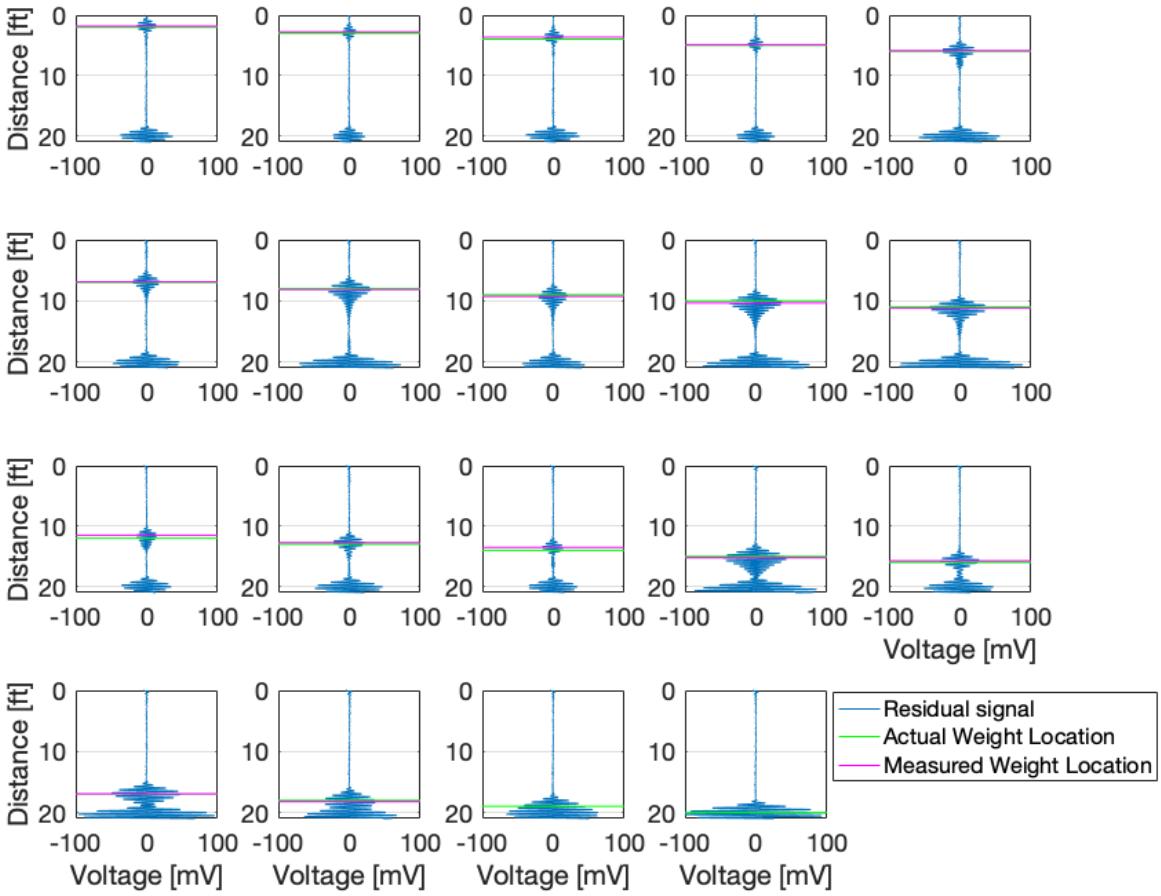

Figure 5. Results from weighted test (every 1 ft) are shown, where measured location was selected as the maximum

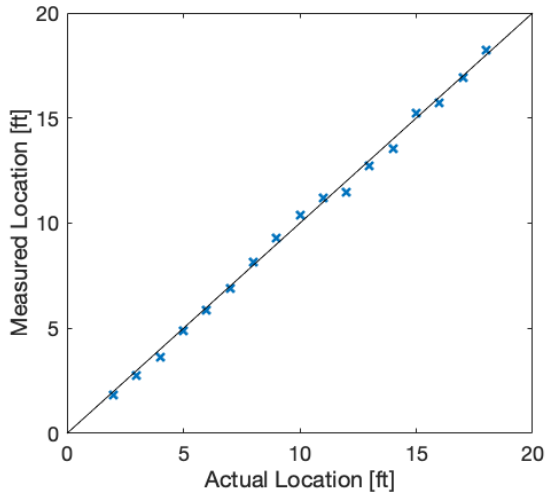

Figure 6. The measured location was selected from a peak-picking algorithm and comparted to the actual location of the weights.

reflection returning from the end of the strip was likely because of energy losses due to the preceding weight reflection. Thus, the measured location was determined by selecting the maximum value of the residual signal that occurred before the appearance of the end-of-strip reflection.

The residual signals from a complete set of localized pressure tests are presented in figure 5. In general, there is a clear change in the residual signal as the position of the weight was moved from 2 to 18 ft. Figure 5 shows the actual location, meaning the location where the weight was placed and diagramed in figure 2a, as a green horizontal line; the location measured by the scour sensor strip based on the maximum residual value is indicated as a horizontal magenta line. The results show that the measured and actual locations coincide well with one another. Further examination of figure 5 shows that the residual signal sees significant changes in voltage amplitude but does not appear to be correlated to the location of the weight. No determination was made as to why the amplitude of the reflected signal fluctuates so significantly based on the location of the weight. This phenomenon is taken into consideration when post-processing the distributed pressure tests in section 4.2.

The accuracy of the scour sensor strip could be better analyzed by comparing and plotting the measured location with respect to the actual location in figure 6. The graph shows a clear trend, and the data was overlaid over the ideal $y=x$ sensor response. None of the reflected packets appeared to

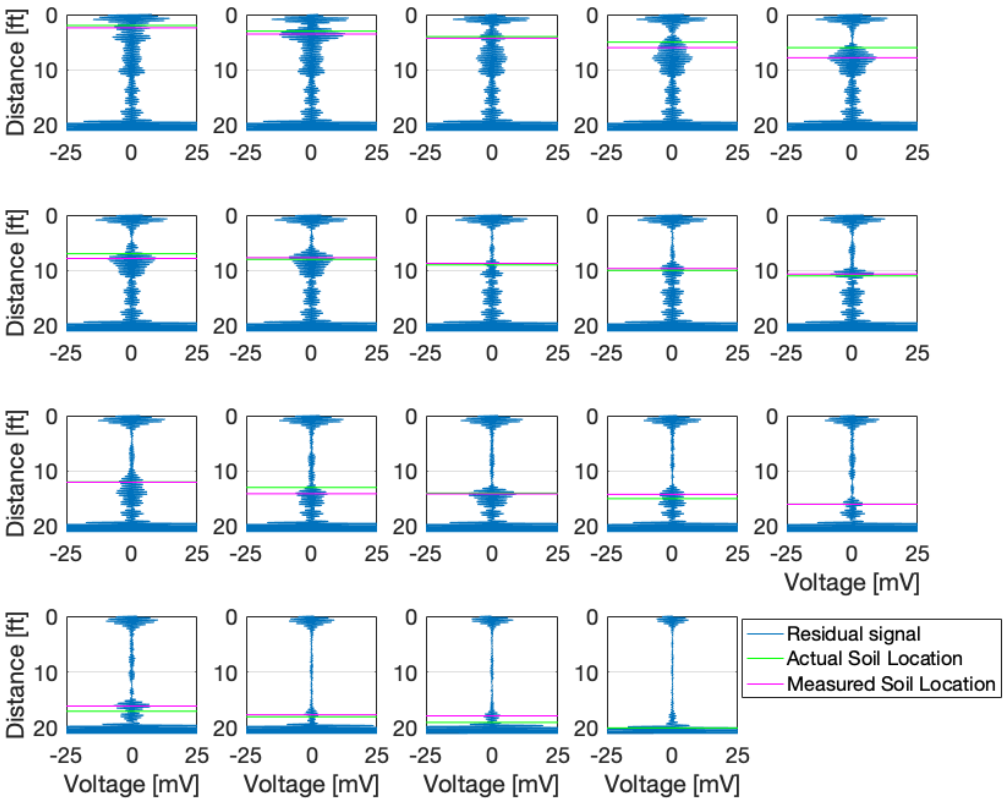

Figure 7. Results from a compacted sand test (every 1 ft) are shown, where measured soil location was chosen using a peak-picking algorithm based on a fraction of the maximum reflected value.

spread significantly, meaning that a dispersive wave propagation was avoided.

4.2 Compacted soil interface

Simulated scour tests, as described in Section 3.4, were performed to verify that the scour sensor strip could detect the leading edge of a distributed pressure interface. As with localized pressure testing, a residual signal was calculated for all locations before further post-processing began.

Due to the complexity of the signals returned from the distributed pressure of a simulated soil interface due to scour, a peak-picking algorithm was used. Oscillations in the residual signal are not compatible with a basic peak picking algorithm. Therefore, to more easily determine the LOI utilizing peak picking, the upper envelope of the signal was calculated. The maximum value of the upper envelope between the input pulse and the first reflection was determined. The maximum value of the upper envelope was not used outright to determine the soil location, as there can be large reflections seen for the duration of the distributed pressure section (*i.e.,* the portion of the strip buried in sand). Instead, a peak threshold of half the maximum value, along with a minimum peak prominence of 0.6 mV, were used for peak selection. Thus, the measured soil interface location was based on the first selected peak with respect to time.

The residual signals produced from the complete set of simulated scour tests are shown in figure 7. The actual location, meaning the end of sand interface and diagramed in figure 2b, is denoted with a horizontal green line; the location measured by the scour sensor is indicated as a horizontal magenta line. The results show that the measured and actual locations coincide well with one another. The largest error is seen at the 6 ft soil-interface location, where the algorithm returned an overestimation of scour at 7.83 ft. The second and third largest errors were at the 13 and 19 ft soil-interface locations, which returned a measured location of 14.1 and 17.8 ft, respectively. Nonetheless, no other locations returned an error larger than 1 ft, suggesting that error is less than 5%. As can be seen in figure 8a, the actual location of the soil-interface aligns well with the corresponding measured location, which is a ground truth location since it is based on the geometry of soil placement. Figure 8a shows a clear trend, and the data was again overlaid over the ideal $y=x$ sensor response. Most errors close to the MFC actuator and sensor are overestimations of the sand interface (or scour depth); underestimations may occur at locations farther away from the excitation and measurement end. Overall, the soil-interface, and therefore the simulated location of scour, was captured within a reasonable range for this technology to be feasible for scour depth monitoring purposes.

As seen in figure 7, a distributed pressure system does not send back a single reflection but rather a series of intermittent pulses along the distributed soil boundary. For a scour sensor,

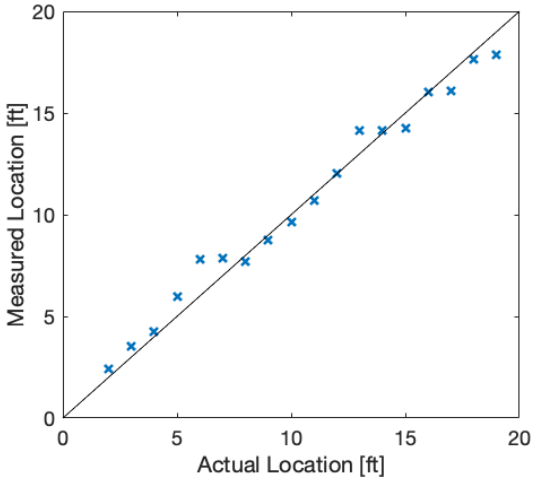

(a)

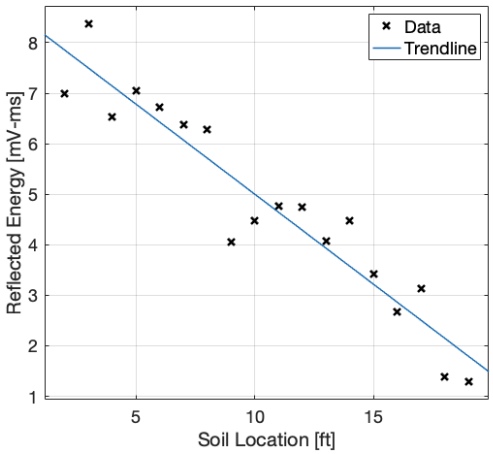

(b)

Figure 8. (a) The measured locations compared to the actual locations of sand show that the sensing mechanism could accurately capture the location of the soil interface. (b) The total reflected energy from the residual signal as scour occurs was calculated by taking the integral of the reflected signal.

this means that reflections would be seen along the total length of the buried portion of the sensor. Therefore, a secondary metric was investigated for identifying the effects of distributed pressure, which was the total reflected energy in the residual signal. The total reflected energy, E_{Rtot}, was calculated by taking an absolute value of the trapezoidal integral of the residual signal written as:

$$E_{Rtot} = \sum_{i=2}^{N} \left| \frac{V(t_{i-1}) + V(t_i)}{2} \right| \Delta t \qquad (2)$$

Where $V(t)$ is the voltage as a function of time, in this case collected as a discrete voltage vector and a corresponding discrete time vector. Therefore, i indicates the index of the row

for both vectors, N is the total number of rows, and Δt is the time step (which in this case is constant).

Figure 8b shows the total reflected energy as a function of the actual soil location. There is an apparent linear downward trend, which is denoted with a blue line. This trend was expected due to the distribution of pressure over the buried length. An increase in the amount of length, and therefore time, over which reflections are occurring would mean a greater amount of total energy reflected. Changes in reflected energy were also notable when examining the raw signals during testing. Typically, six or more end-of-strip reflections could be seen from an unburied sensor. However, on sensors with most of their length buried, no end-of-strip reflections were visible. Figure 8b indicates that the relationship between the reflected energy and the soil-interface does not show the precision necessary to pinpoint scour location based on the reflected energy alone. However, the total reflected energy does give a nominal amount of insight into the effects of the surrounding sediment on the sensor, which will be explored further in section 4.3.

4.3 Uncompacted soil interface

Uncompacted soil interface tests, also described in section 3.4, were performed to study the capability of the scour sensor strip to identify the location of the sand interface under non-ideal conditions. As previously stated, scour can produce periods of erosion as well as infill. The results that follow are an indication of the scour sensor's ability to perform under simulated infill conditions, where infilled sediments are less compacted than before when scour occurred.

The residual signals from the uncompacted soil test are shown in figure 9. As with the other residual signals, the actual soil interface location is denoted with a horizontal green line; the measured location is marked with a magenta line. In three out of the four cases, the measured location for uncompacted sand was detected near the compacted sand location.

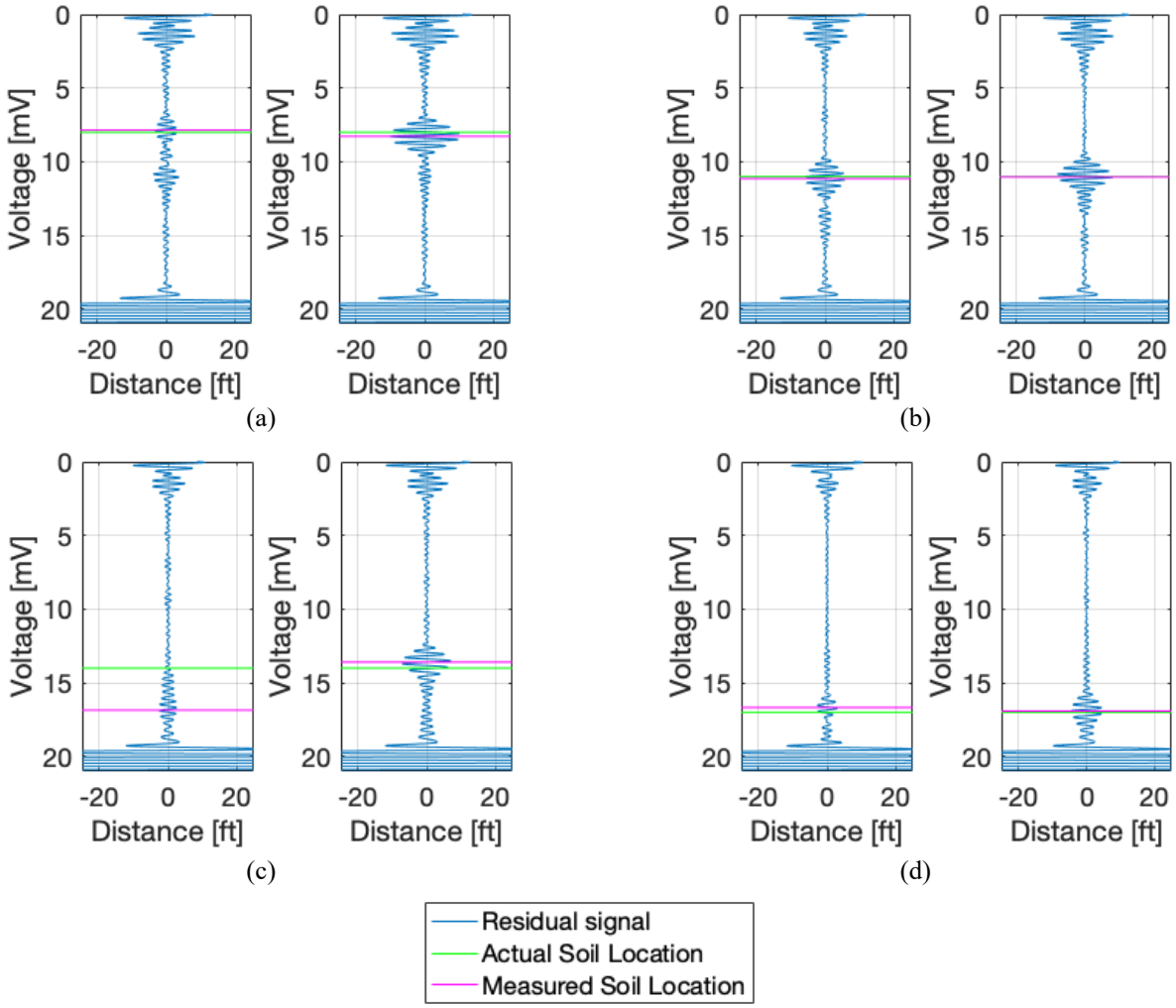

Figure 9. The raw signals were captured from uncompacted (left) and compacted sand (right) at (a) 8, (b) 11, (c) 14, and (d) 17 ft locations.

Table 1: Measurement errors calculated as the mean (M) and standard deviations (SD) of error

	Measurement Error [ft]	
	M	SD
Localized Pressure (weight)	0.25	0.12
Simulated Scour	0.59	0.48
Compacted Sand	0.20	0.17
Uncompacted Sand	0.87	1.32

Furthermore, for all four cases, the compacted sand location was measured to be within 0.5 ft of the LOI.

For the 14 ft location, figure 9c shows that the scour sensor failed to detect the additional uncompacted sand that was added. Instead, the sensor returned a location very near the previously detected compacted sand location of 17 ft. However, after examining the signal visually, there appears to be the formation of a small pulse with a leading edge near the location of the sand interface, so further testing is needed to adjust the sensitivity appropriately. A comparison of the measured locations and the actual locations for the compaction tests are shown in figure 10a, again showing the ideal $y=x$ sensor case. Overall, the scour sensor showed the ability to detect both compacted and uncompacted sand interfaces with reasonable accuracy.

Interestingly, the residual signals show a difference to those seen during the 1 ft interval simulated scour testing. Clearly, the signals in figure 9 do not show as many trailing pulses following the LOI as do the residual signals in figure 7. This is hypothesized to be because of the way that sand was added, as this is the only significant difference between these two tests. Ideally, this would mean that the UTDR technique will perform well in the field, where the distribution of sand or other soil pressure is even (as it is not added in small portions) and a clear leading pulse will dominate the signal signature. More tests are needed in the future to confirm this hypothesis.

The total reflected energy was also evaluated for both the uncompacted and compacted residual signals (figure 10b). As expected, the compacted sand at any given location has a higher amount of reflected energy than its uncompacted counterpart. This makes the classification of sand or other soil compaction probable with the UTDR method once the soil interface location is determined using TOF, or if the location is known *a priori*.

The accuracy of the scour sensor in all four test cases is compared in table 1, where the mean and standard deviations of error – the absolute difference between the ideal $y=x$ case

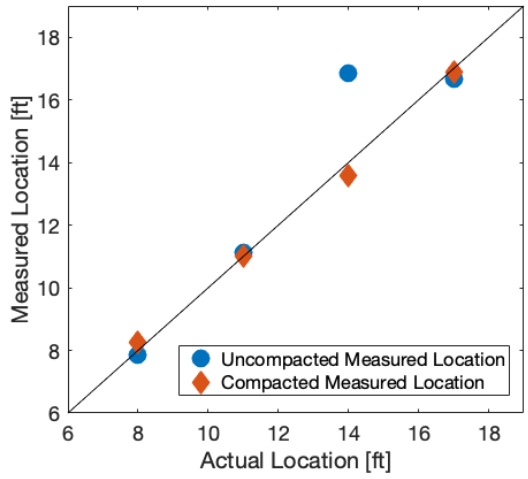

(a)

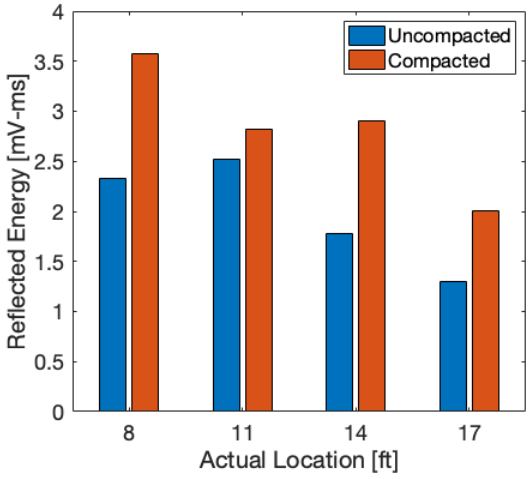

(b)

Figure 10. (a) Compacted and uncompacted soil interfaces are both measured by UTDR. (b) The total reflected energy from the integral of the residual was related to the level of compaction.

and the acquired measurement – are given. The table shows that the localized pressure detection is most accurate, which is expected. Simulated scour has a mean error below 1ft, even with the presence of the trailing pulses seen with distributed pressure. The compacted sand test, like simulated scour except for the intervals at which sand was applied, showed accuracy in a similar range to the localized pressure testing. This is very encouraging because, as stated earlier, soil in the field will likely not see as many trailing pulses because sediment is deposited with more even pressure. Furthermore, as expected, the uncompacted sediment has the lowest accuracy, and shows a higher standard deviation due to the missed measurement of the 14-foot location.

Compared to the most recent work on an electrical TDR system, which has an estimated maximum error of 0.6 ft (0.19

m) [23], the UTDR Lamb wave method sees almost three times the maximum error in its current iteration (*i.e.*, excluding the outlier observed at 14 ft in the uncompacted test). However, there are significant differences in the maturity of the two technologies, and this level of accuracy was not achieved until 2020. The average error of the proposed UTDR is below the 5% average error expected from earlier iterations of the electrical TDR sensor as discussed in Yankielun and Zabilansky (1999), Lin *et al*. (2017), and Yu *et al.* (2020) [17,20,21].

4.4 Considerations for field deployment

Since this study was focused on validating the UTDR method for scour monitoring, there are steps beyond this work that is needed to develop a UTDR scour sensor ready for field deployment. Some of the next steps are discussed as follows:

(1) Testing conditions: The scour sensor used in this study was tested horizontally, since the strip was not rigid enough to hold itself vertically. During this study, it was found that flexion in the strip could introduce unwanted signatures in the residual signal. This might be solved by placing the strip sensor in tension close to the pier, as was done with ETDR sensors [22]. Futhermore, testing was only done using sand as the soil medium. Other tests should be performed to validate the UTDR sensors' ability to detect other soil interfaces (*i.e.* clay, silt, etc.)

(2) Physical properties: In the case of a standalone scour sensor design, a more robust strip that does not buckle or bend under self-weight would need to be developed. Based on studies by Funderburk *et al.* [38,39] as well as Azhari and Loh [40], standalone scour sensors that are exposed to flowing water will undergo vortex-induced vibrations, which may also be a source of flexion.

(3) MFC sensor and actuator: It is also possible to use only one MFC as both the sensor and the actuator, which would be more cost effective for large-scale deployment. Furthermore, a steel sensing strip is susceptible to corrosion, which over time would undoubtedly damage or destroy the sensor.

(4) Environmental protection: The MFC sensor and actuator are not waterproofed or protected from environmental damage. This can be addressed by bonding and protecting the MFCs with epoxy, but more studies are needed to determine how they affect Lamb wave propagation.

(5) Environmental effects: As with any sensor, some sensitivities to outside environmental effects may occur. Changes in water temperature could cause expansion or contraction of the metal sensing strip, which would change the propagation speed of the Lamb wave and cause inaccuracies in soil interface location detection. Depending on the type of sensor developed (either standalone or adjacent to a pier), temperature changes could be uneven above and below the water surface.

5. Conclusions

This study tests the hypothesis that the Lamb wave UTDR method using a long, slender, and thin steel strip could detect a soil interface for the purposes of scour monitoring. First, scour sensor tests were performed using weights to produce a localized pressure interface. The results showed that the Lamb wave UTDR method could be used to detect external applied pressure interfaces along the steel strip and up to 21 ft in length. Second, a laboratory experiment that simulated scour conditions performed were performed using a soil box, where large portions of the scour sensor could be completely buried in sand. The scour sensor was able to detect the sand interface of a buried sensor with a high level of accuracy, with an average of less than 1 ft of error. The scour sensor was also tested with uncompacted sand interfaces, and it was able to detect these looser interfaces in three out of four test cases. By analyzing the total reflected energy in the residual signals, it was found that uncompacted sand consistently returned less energy than compacted sand at the same level. Therefore, the sensor could potentially provide feedback on the soil compaction level, which could help to identify the presence of compromised foundations that appear sufficient, assuming that the depth of soil has been determined or is known. Overall, the novel Lamb wave UTDR method showed that it could accurately detect the location of the soil-interface of a buried strip for the purposes of scour monitoring.

Acknowledgements

This research was supported by the U.S. Army Corps of Engineers (USACE) Cooperative Research Agreement No. W912HZ-17-2-0024. The authors acknowledge Mr. A. Drew Barnett and Dr. Joseph Reed from Elintrix, who are close collaborators and consulted on various aspects of this project. The authors also gratefully acknowledge Dr. Francesco Lanza di Scalea and his laboratory who kindly lent us the high-frequency amplifier used during ultrasonic tests.

References

[1] Pizarro, Manfreda and Tubaldi 2020 The Science behind Scour at Bridge Foundations: A Review *Water* **12** 374

[2] Melville B W 1975 *Local Scour at Bridge Sites*

[3] Richardson E V and Richardson J R 1989 *Bridge Scour*

[4] Montalvo C, Cook W and Keeney T 2020 Retrospective Analysis of Hydraulic Bridge Collapse *J. Perform. Constr. Facil.* **34** 2–9

[5] Arneson L A, Zevenbergen L W, Lagasse P F and Clopper P E 2012 Evaluating Scour at Bridges. HEC-18. Fifth Edition, Hydraulic Engineering Circular No. 18. Publication *No. FHWA-HIF-12-003. U.S. Dep. Transp. Fed. Highw. Adm.* 340

[6] American Association of State Highway and Transportation Officals 2010 *AASHTO LRFD Bridge Design Specifications*

[7] U.S Department of the Interior and Survey U S G 2000 *Measuring Scour of the Streambed at Highway Bridges* vol FS 107-00

[8] Neumann J E, Price J, Chinowsky P, Wright L, Ludwig L, Streeter R, Jones R, Smith J B, Perkins W, Jantarasami L and Martinich J 2015 Climate change risks to US infrastructure: impacts on roads, bridges, coastal development, and urban drainage *Clim. Change* **131** 97–109

[9] Demirel H 2012 *Impacts of Climate Change on Transport: A focus on road and rail transport infrastructures Impacts of Climate Change: A focus on road and rail transport infrastructures Françoise Nemry, Hande Demirel 2 0 1 2*

[10] De Falco F and Mele R 2002 The monitoring of bridges for scour by sonar and sedimetri *NDT E Int.* **35** 117–23

[11] Lin Y Bin, Chen J C, Chang K C, Chern J C and Lai J S 2005 Real-time monitoring of local scour by using fiber Bragg grating sensors *Smart Mater. Struct.* **14** 664–70

[12] Huang L, Wang D and Zhou Z 2007 A New Type of Optical FBG-based Scour Monitoring sensor **9** 103–9

[13] Kong X, Ho S C M, Song G and Cai C S 2017 Scour Monitoring System Using Fiber Bragg Grating Sensors and Water-Swellable Polymers *J. Bridg. Eng.* **22** 1–11

[14] Ding Y, Yao Q, Zhang Z, Wang X, Yan T, Yang Y and Lv H 2018 A new method for scour monitoring based on fiber Bragg grating *Meas. J. Int. Meas. Confed.* **127** 431–5

[15] Zarafshan A, Iranmanesh A and Ansari F 2012 Vibration-based method and sensor for monitoring of bridge scour *J. Bridg. Eng.* **17** 829–38

[16] Zhao X, Li L and Yu Y Fiber Optical Scour Monitoring System for Subsea Oil Pipe Line

[17] Yankielun N E and Zabilansky L 1999 Laboratory Investigation of Time-Domain Reflectometry System for Monitoring Bridge Scour **125** 1279–84

[18] Yu X and Yu X 2010 Laboratory evaluation of Time-Domain Reflectometry for bridge scour measurement: Comparison with the ultrasonic method *Adv. Civ. Eng.* **2010**

[19] Yu X and Yu X 2009 Time domain reflectometry automatic bridge scour measurement system: Principles and potentials *Struct. Heal. Monit.* **8** 463–76

[20] Yu J D, Lee J S and Yoon H K 2020 Circular time-domain reflectometry system for monitoring bridge scour depth *Mar. Georesources Geotechnol.* **38** 312–21

[21] Lin C P, Wang K, Chung C C and Weng Y W 2017 New types of time domain reflectometry sensing waveguides for bridge scour monitoring *Smart Mater. Struct.* **26**

[22] Wang K, Lin C P and Chung C C 2019 A bundled time domain reflectometry-based sensing cable for monitoring of bridge scour *Struct. Control Heal. Monit.* **26** 1–14

[23] Wang K and Lin C P 2021 Applicability and limitations of time domain reflectometry bridge scour monitoring system in general field conditions *Struct. Heal. Monit.* **20** 1074–89

[24] Munian R K, Mahapatra D R and Gopalakrishnan S 2018 Lamb wave interaction with composite delamination *Compos. Struct.* **206** 484–98

[25] Zhao J, Durham N, Abdel-Hadi K, McKenzie C A and Thomson D J 2019 Acoustic guided wave techniques for detecting corrosion damage of electrical grounding rods *Meas. J. Int. Meas. Confed.* **147** 106858

[26] An Y K, Kim J H and Yim H J 2014 Lamb wave line sensing for crack detection in a welded stiffener *Sensors (Switzerland)* **14** 12871–84

[27] Funderburk M, Todd M D, Netchaev A and Loh K J 2021 Active scour monitoring using ultrasonic time-domain reflectometry to detect a soil interface **1159113** 36

[28] Bolduc L C, Gardoni P and Briaud J L 2008 Probability of exceedance estimates for scour depth around bridge piers *J. Geotech. Geoenvironmental Eng.* **134** 175–84

[29] Kundu T and Maslov K 1997 Material interface inspection by Lamb waves *Int. J. Solids Struct.* **34** 3885–901

[30] Rathod V T, Mahapatra D R, Jain A and Gayathri A 2010 Characterization of a large-area PVDF thin film for electro-mechanical and ultrasonic sensing applications *Sensors Actuators, A Phys.* **163** 164–71

[31] Alleyne D N and Cawley P 1992 The Interaction of Lamb Waves with Defects *IEEE Trans. Ultrason. Ferroelectr. Freq. Control* **39** 381–97

[32] Volker A and Bloom J 2011 Experimental results of guided wave travel time tomography *AIP Conf. Proc.* **1335** 215–22

[33] Atashipour S A, Mirdamadi H R, Hemasian-Etefagh M H, Amirfattahi R and Ziaei-Rad S 2013 An effective damage identification approach in thick steel beams based on guided ultrasonic waves for structural health monitoring applications *J. Intell. Mater. Syst. Struct.* **24** 584–97

[34] Alleyne D N and Cawley P 1992 Optimization of lamb wave inspection techniques *NDT E Int.* **25** 11–22

[35] Sodano H A, Park G and Inman D J 2004 An investigation into the performance of macro-fiber composites for sensing and structural vibration applications *Mech. Syst. Signal Process.* **18** 683–97

[36] Mańka M, Rosiek M, Martowicz A, Stepinski T and Uhl T 2013 Lamb wave transducers made of piezoelectric macro-fiber composite *Struct. Control Heal. Monit.*

[37] Shull P J 2001 *Nondestructive Evaluation* (Boca Raton: CRC Press)

[38] Funderburk M L, Huang S-K, Loh C-H and Loh K J 2019 Densely distributed and real-time scour hole monitoring using piezoelectric rod sensors *Adv. Struct. Eng.* **22** 3395–411

[39] Funderburk M L, Park Y, Netchaev A and Loh K J 2021 Piezoelectric rod sensors for scour detection and vortex-induced vibration monitoring 1–15

[40] Azhari F and Loh K J 2017 Laboratory validation of buried piezoelectric scour sensing rods *Struct. Control Heal. Monit.* **24** 1–14